Heteroatom Chemistry
Volume 22, Number 3/4, 2011

Effects of Heterole Spacers on the Structural, Optical, and Electrochemical Properties of 2,5-Bis(1,5-diphenylphosphol-2-yl)heteroles

Yoshihiro Matano,[1] Arihiro Saito,[1] Masato Fujita,[1] and Hiroshi Imahori[1–3]

[1]*Department of Molecular Engineering, Graduate School of Engineering, Kyoto University, Nishikyo-ku, Kyoto 615-8510, Japan*

[2]*Institute for Integrated Cell-Material Sciences (iCeMS), Kyoto University, Nishikyo-ku, Kyoto 615-8510, Japan*

[3]*Fukui Institute for Fundamental Chemistry, Kyoto University, Sakyo-ku, Kyoto 606-8103, Japan*

Received 31 August 2010; revised 21 November 2010

ABSTRACT: *2,5-Bis(1,5-diphenylphosphol-2-yl)heterole derivatives were prepared via Pd-catalyzed Stille-type cross-coupling reactions of α-(tributylstannyl) phosphole or α-iodophosphole with the corresponding 2,5-difunctionalized heteroles (pyrrole, furan, and thiophene). X-ray crystallographic analyses of three σ^4-P derivatives have elucidated that the coplanar phosphole-heterole-phosphole π-networks are constructed in both anti–anti and syn–anti conformations. In the case of the pyrrole-linked σ^4-P derivatives, there is a weak hydrogen-bonding interaction between NH and P=X (X = O, S) groups. The optical and electrochemical properties of the σ^3-P and σ^4-P=O derivatives were revealed experimentally by means of UV–vis absorption/emission spectroscopy and cyclic/differential pulse voltammetry. In all the heterole-linked derivatives, the P-oxidation lowers LUMO levels more efficiently than HOMO levels and, as a result, narrows HOMO–LUMO gaps. In each series (σ^3-P or σ^4-P=O), the lowest π–π* transition energies of the phosphole–heterole–phosphole π-systems were found to decrease in the following order: thiophene > furan > pyrrole, and their electrochemical oxidation and reduction potentials shift to the negative side in the same order. These results basically reflect the differences in ionization potential and electron affinity of the central heterole spacers. Density functional theory calculations on the model compounds supported the experimentally observed results. The HOMO of the molecule resides on the conjugated polyene network of the π-system, whereas the LUMO is strongly located on the phosphole subunits. The present comparative study demonstrates, for the first time, that the intriguing electronic structures and the fundamental properties of the 2,5-bis(1,5-diphenylphosphol-2-yl)heteroles can be finely tuned by simple selection of the appropriate heterole spacer.* © 2011 Wiley Periodicals, Inc. Heteroatom Chem 22:457–470, 2011; View this article online at wileyonlinelibrary.com. DOI 10.1002/hc.20708

INTRODUCTION

Phosphole is now regarded as a promising constituent for making π-conjugated organic materials

Dedicated to Professor Kin-ya Akiba on the occasion of his 75th birthday.

Correspondence to: Yoshihiro Matano; e-mail: matano@scl.kyoto-u.ac.jp.

Contract grant sponsor: Grants-in-Aid from the Ministry of Education, Culture, Sports, Science and Technology, Japan.
Contract grant number: 21108511.
Contract grant sponsor: Asahi Glass Foundation.
Contract grant number: 22350016.

with a low-lying LUMO, a narrow HOMO–LUMO gap, and a polarizable dienic unit [1]. These characteristic properties of phosphole are derived from effective σ^*–π^* orbital interaction between the phosphorus center and the adjacent 1,3-diene unit. Therefore, chemical functionalizations at the phosphorus and α-carbon atoms of the phosphole ring are promising strategies to control the optoelectronic properties of phosphole-containing π-systems.

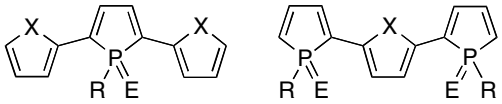

A (X = heteroatom) **B** (X = heteroatom)

Heterole–phosphole–heterole hybrid π-systems of general formula A [2,5-bis(2-heterolyl)phospholes], especially those bearing 2-thienyl groups, have been extensively studied, and their fundamental properties have proven to correlate well with the character of the α-substituents [2–5]. In these compounds, the central phosphole subunit provides a π-spacer framework to enable conjugative connectivity to adjacent heterole moieties. In contrast, the number of phosphole–heterole–phosphole π-systems of general formula B [2,5-bis(2-phosphoryl)heteroles] is rather limited as compared with that of type A derivatives.

Figure 1 depicts a few examples of type B compounds reported previously. Mathey and co-workers reported a multistep synthesis of **K-1** and **K-2** via Friedel–Crafts C—C bond-forming reactions of 3,4-dimethylphosphole P-metal complexes with the respective heteroles and disclosed a crystal structure

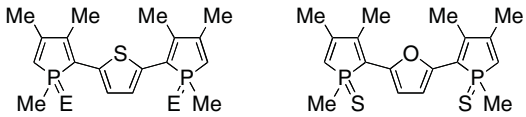

K-1 (E = lone pair, S)

K-2

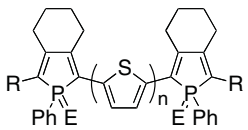

K-3 (*n* = 1, 2; E = lone pair, S; R = 2-thienyl, 2-pyridyl)

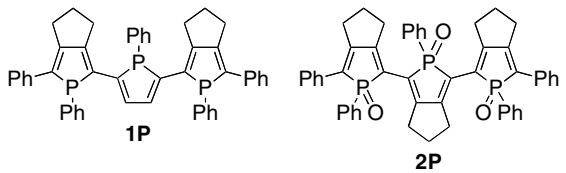

1P **2P**

FIGURE 1 Examples of 2,5-bis(phosphoryl)heteroles.

of **K-1** ($E = S$) [6]. To our knowledge, however, optical and electrochemical properties of **K-1** and **K-2** have not been discussed in the literature. Réau and co-workers reported the optical, electrochemical, and electroluminescent properties of thiophene- and bithiophene-linked phosphole derivatives **K-3**, which had been prepared by the Fagan–Nugent method from the corresponding thiophene–acetylene precursors [7]. Importantly, both types A and B phosphole derivatives can be regarded as the smallest units of phosphole–heterole π-conjugated oligomers and polymers, which have received increasing attention in the search of potential candidates for the phosphorus-based optoelectrochemical materials [8]. In this context, it is of significance to understand electronic and steric effects of the heterole spacers on the fundamental properties of type B phosphole derivatives. Recently, we reported the first examples of α,α'-linked terphospholes **1P** [9] and **2P** [10] (Fig. 1), which exhibited considerably narrow HOMO–LUMO gaps derived from the phosphole–phosphole–phosphole linkage. In this study, we aimed to establish a convenient method for the construction of phosphole–heterole–phosphole (heterole: pyrrole, furan, thiophene) linkages and to elucidate intrinsic effects of these heterole spacers on the fundamental properties of type B phosphole derivatives. We report, herein, a new synthesis of three classes of 2,5-bis(1,5-diphenylphosphol-2-yl)heteroles **1X** and **2X** (**X = N, O, S**) based on the Pd-catalyzed cross-coupling method. With a series of type B compounds available, we have comparatively elucidated the effects of the heterole-spacers on the structural, optical, and electrochemical properties of the phosphole–heterole–phosphole π-systems.

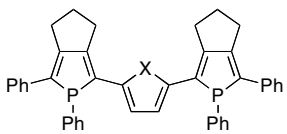

1X

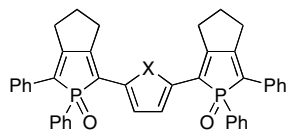

2X

(X = NH, O, S)

RESULTS AND DISCUSSION

Synthesis of 2,5-Bis(1,5-diphenylphosphol-2-yl)heteroles

Scheme 1 illustrates the synthesis of 2,5-bis(1,5-diphenylphosphol-2-yl)heterole P-oxide derivatives **2X**. The starting materials α-iodophosphole **3** and α-(tributylstannyl)phosphole **4** were prepared according to the reported procedure [10]. Both of

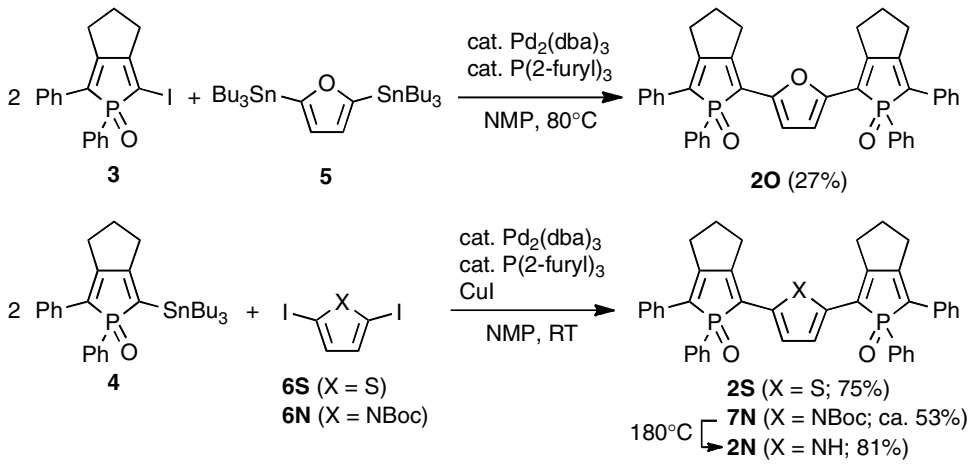

SCHEME 1 Synthesis of σ^4-P=O derivatives **2X**.

these functionalized phospholes have proven to be promising synthons in cross-coupling reactions [10]. Treatment of **3** with 2,5-bis(tributylstannyl)furan **5** in the presence of $Pd_2(dba)_3$ and P(2-furyl)$_3$ in NMP for 47 h at 80°C afforded phosphole–furan–phosphole P-oxide **2O** as the major product. The low-yield formation of **2O** was attributable in a part to an occurrence of a side reaction, homocoupling of **5** under the reaction conditions employed. Phosphole–thiophene–phosphole P-oxide **2S** and phosphole–Boc–pyrrole–phosphole P-oxide **7N** (Boc = *tert*-butoxycarbonyl) were prepared by the Pd-CuI-promoted Stille-type reaction between α-(tributylstannyl)phosphole **4** and the corresponding 2,5-diiodoheteroles **6X** (**X = S, N**). Under the Pd-CuI reaction conditions, **4** was consumed within 2 h at room temperature, although the formation of a small amount of α,α'-biphosphole, namely a homocoupling product of **4**, could not be suppressed completely. When heated at 180°C for 30 min without solvent, the Boc group of **7N** was successfully deprotected to afford **2N** in 81% yield. Compounds **2O, 2S, 2N**, and **7N** possess two chiral centers at phosphorus, and were obtained as a mixture of two diastereomers. The diastereoselectivity of the cross-coupling reaction (major/minor) was found to be 62/38 for **2O**, 65/35 for **2S**, and 62/38 for **7N** (determined by ^{1}H and ^{31}P NMR). The diastereomers of **2O** and **7N** were successfully separated from each other by a combination of recrystallization and column chromatography, but those of **2S** were difficult to separate by these methods because of the low solubility. Compound **2N** was obtained as a single diastereomer from one of the diastereomers of **7N**, by retention of the stereochemistry at phosphorus.

Reductive deoxygenation at the phosphorus centers of **2O** and **2S** (each a mixture of diastereomers) was achieved with trichlorosilane in chloroform to give **1O** and **1S**, respectively (Scheme 2). Compound **1O** was isolated in 74% yield by recrystallization, whereas **1S** was isolated in 44% yield by column chromatography. The σ^4-P=O centers of **7N** were also reduced in the same manner, by treatment with excess trichlorosilane. However, it was found that the Boc group of the resulting σ^3-P product could not be removed cleanly under our reaction conditions (NaOMe in THF-MeOH, reflux, 21 h). Hence, we decided to synthesize the pyrrole-linked σ^3-P derivative **1N** via P-sulfide **8N**. Heating a mixture of **7N** and Lawesson's reagent in toluene afforded the phosphole–pyrrole–phosphole P-sulfide **8N** accompanied by simultaneous deprotection of the N-Boc group. The reductive desulfurization of **8N** proceeded smoothly by reflux with excess P(NMe$_2$)$_3$ in toluene to produce the target compound **1N** in good yield. In contrast to the σ^4-P derivatives **2X**, two diastereomers of the σ^3-P derivatives **1X** were

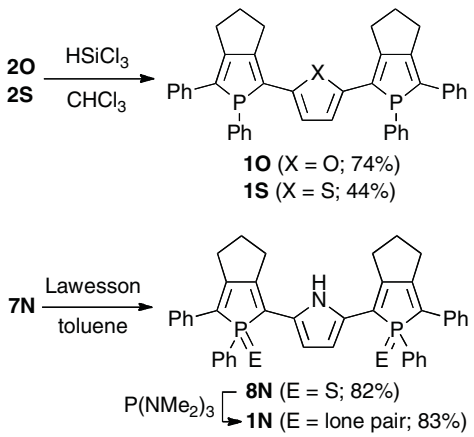

SCHEME 2 Synthesis of σ^3-P derivatives **1X**.

not separable from each other, suggesting that the pyramidal inversion occurs at the phosphorus centers for **1X** [11]. Indeed, two sets of ^{1}H peaks due to the furan-β protons of **1O** coalesced at 75°C in $Cl_2CDCDCl_2$. It should be noted here that the same diastereomeric mixtures of **1O** and **1N** were obtained from **2O** and **8N**, respectively. These results imply that there is very little difference in the thermodynamic stability between two diastereomers of **1X**.

Characterization of 2,5-Bis(1,5-diphenylphosphol-2-yl)heteroles

The newly prepared phosphole-heterole-phosphole π-systems, 2,5-bis(1,5-diphenylphosphol-2-yl)heterole derivatives **1X, 2X, 7N**, and **8N**, were characterized by standard spectroscopic techniques (^{1}H, ^{31}P NMR, high-resolution MS, IR) and X-ray crystallography (for **2O, 2N**, and **8N**). In the ^{31}P NMR spectra of the diastereomeric mixtures in $CDCl_3$, a set of two singlet peaks with similar intensity was observed at δ_P 29.3–33.7 ppm for **1X** and δ_P 52.5–54.2 ppm for **2X**. The differences in δ_P values between two diastereomers of **1X** and **2X** were found to be very small ($\Delta\delta_P < 0.4$ ppm). The ^{31}P chemical shifts observed for a series of the pyrrole-linked derivatives **1N** (δ_P 29.3, 29.6 ppm), **2N** (δ_P 54.2 ppm for one diastereomer), and **8N** (δ_P 64.5, 65.9 ppm) represent the intriguing nature of the relevant phosphorus centers. In the ^{1}H NMR spectra, all the diastereomers of **1X** and **2X** displayed symmetrical spectral patterns owing to C_s or C_2 symmetry, indicating that the rotation at the interring carbon–carbon bonds takes place rapidly on the NMR time scale. The reduction at the phosphorus center from σ^4-P=O (**2X**) to σ^3-P (**1X**) induces noticeable upfield shifts of the heterole-β protons by 0.25–0.43 ppm. This implies that the changes in hybridization mode and electron density at the phosphorus atoms are strongly reflected in the electronic character of the central heterole subunits through the π-network. In the ^{1}H NMR spectra of P-oxide **2N** and P-sulfide **8N** in $CDCl_3$, the NH protons were observed at δ_H 9.75 ppm (one diastereomer) and 10.20/10.24 ppm (a mixture of diastereomers), respectively. The downfield appearances of the NH peaks of **2N** and **8N** relative to those of **1N** (δ_H 7.96/8.04 ppm) indicate that the NH protons of these σ^4-P derivatives receive spatial electronic influences from the neighboring P=O or P=S groups. In other words, hydrogen-bonding interaction operates between the NH protons and the oxygen/sulfur atoms bound to phosphorus in **2N** and **8N** (vide infra). The degree of downfield shifts of the NH peaks observed for the present phosphole–pyrrole–phosphole π-systems ($\Delta\delta_{NH}$ = 1.71–1.79/2.16–2.28 ppm; **2N**/**8N** relative to **1N**) is larger than that reported for the pyrrole–phosphole–pyrrole π-systems ($\Delta\delta_{NH}$ = 1.02/1.70 ppm; σ^4-P=O/P=S relative to σ^3-P) [5]. The fact that $\Delta\delta_{NH}$ values vary depending on the ratio of NH/P=X groups may support the above interpretation.

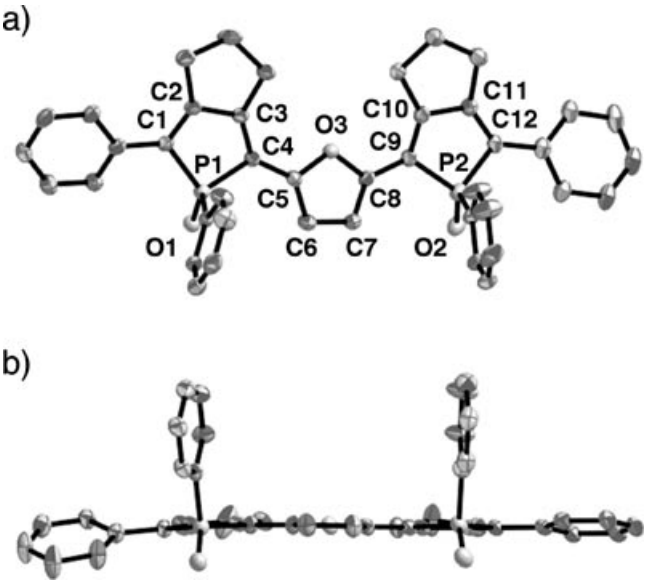

FIGURE 2 (a) Top view and (b) side view of **2O** (30% probability ellipsoids). Hydrogen atoms are omitted for clarity. Selected bond lengths (Å) and angles (°): C(1)–C(2), 1.366(6); C(2)–C(3), 1.481(6); C(3)–C(4), 1.353(6); C(4)–C(5), 1.427(6); C(5)–C(6), 1.364(6); C(6)–C(7), 1.406(6); C(7)–C(8), 1.377(6); C(8)–C(9), 1.430(6); C(9)–C(10), 1.362(5); C(10)–C(11), 1.470(6); C(11)–C(12), 1.350(6); P(1)–C(1), 1.835(4); P(1)–C(4), 1.827(4); P(1)–O(1), 1.480(3); P(2)–C(9), 1.812(4); P(2)–C(12), 1.830(4); P(2)–O(2), 1.492(3); C(1)–P(1)–C(4), 93.68(19); O(1)–P(1)–C(1), 118.84(19); O(1)–P(1)–C(4), 117.87(18); C(9)–P(2)–C(12), 94.13(19); O(2)–P(2)–C(9), 116.37(18); O(2)–P(2)–C(12), 119.26(18).

The structures of **2O, 2N**, and **8N** (each, one of the diastereomers) were further elucidated by X-ray crystallography (Figs. 2–4). In the furan-linked derivative **2O**, both of the phosphole rings adopt S-trans (anti) conformation against the furan ring, and two P-phenyl groups are nonalternated. The distortion between the central furan and adjacent phosphole rings is very little (dihedral angles, α = 177.7°and 175.9°), which implies that the phosphole–furan–phosphole π-system is effectively conjugated. In the pyrrole-linked derivatives **2N** and **8N**, one phosphole ring adopts S-trans (anti) conformation against the pyrrole ring, whereas the other adopts S-cis (syn) conformation. Based on this

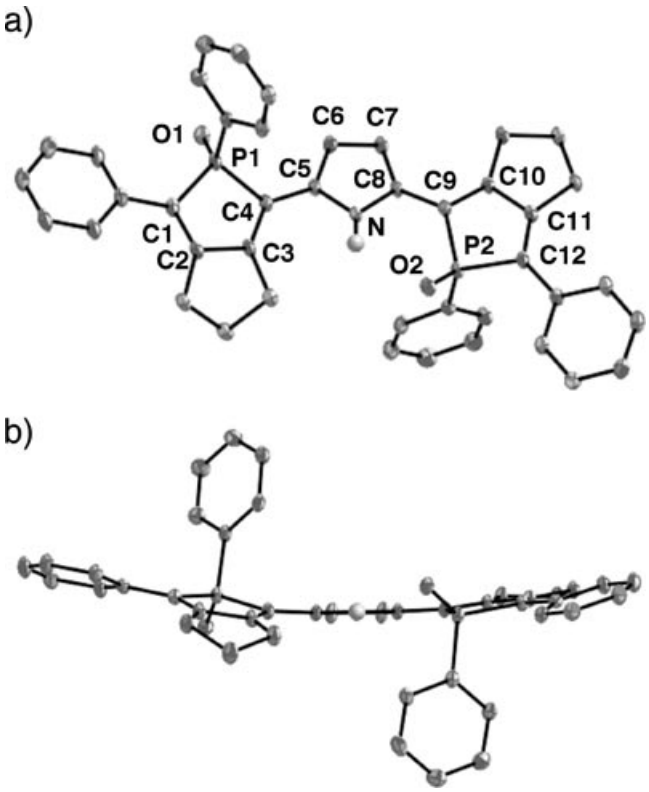

FIGURE 3 (a) Top view and (b) side view of **2N** (30% probability ellipsoids). Hydrogen atoms except for NH are omitted for clarity. Selected bond lengths (Å) and angles (°): C(1)–C(2), 1.351(4); C(2)–C(3), 1.488(4); C(3)–C(4), 1.360(4); C(4)–C(5), 1.440(4); C(5)–C(6), 1.384(4); C(6)–C(7), 1.403(4); C(7)–C(8), 1.385(4); C(8)–C(9), 1.437(4); C(9)–C(10), 1.358(4); C(10)–C(11), 1.476(4); C(11)–C(12), 1.360(4); P(1)–C(1), 1.820(3); P(1)–C(4), 1.809(3); P(1)–O(1), 1.491(2); P(2)–C(9), 1.813(3); P(2)–C(12), 1.826(3); P(2)–O(2), 1.488(2); C(1)–P(1)–C(4), 93.88(14); O(1)–P(1)–C(1), 116.24(14); O(1)–P(1)–C(4), 117.66(14); C(9)–P(2)–C(12), 94.35(14); O(2)–P(2)–C(9), 114.83(14); O(2)–P(2)–C(12), 121.62(14).

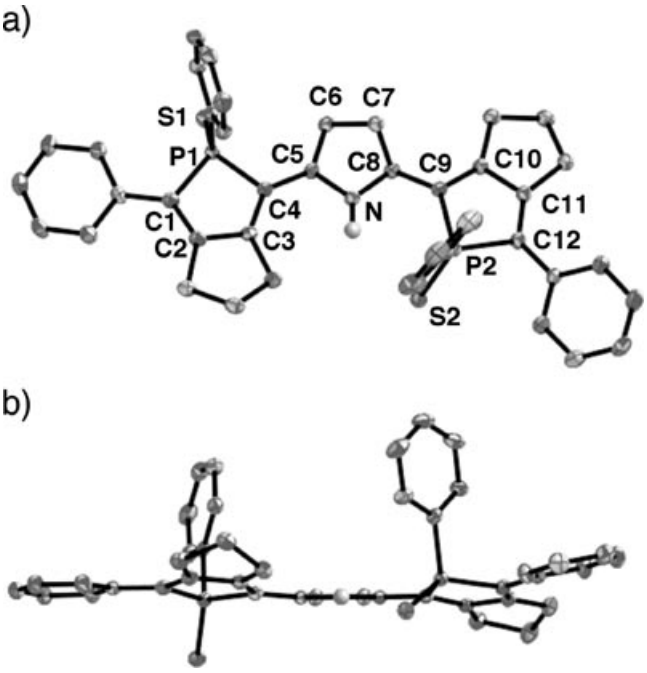

FIGURE 4 (a) Top view and (b) side view of **8N** (30% probability ellipsoids). Hydrogen atoms except for NH are omitted for clarity. Selected bond lengths (Å) and angles (°): C(1)–C(2), 1.352(5); C(2)–C(3), 1.461(5); C(3)–C(4), 1.354(4); C(4)–C(5), 1.422(4); C(5)–C(6), 1.375(5); C(6)–C(7), 1.393(5); C(7)–C(8), 1.384(4); C(8)–C(9), 1.434(4); C(9)–C(10), 1.350(4); C(10)–C(11), 1.455(4); C(11)–C(12), 1.364(5); P(1)–C(1), 1.828(3); P(1)–C(4), 1.819(3); P(1)–S(1), 1.9486(13); P(2)–C(9), 1.807(3); P(2)–C(12), 1.822(3); P(2)–S(2), 1.9580(13); C(1)–P(1)–C(4), 93.99(15); S(1)–P(1)–C(1), 117.61(11); S(1)–P(1)–C(4), 117.19(11); C(9)–P(2)–C(12), 94.24(15); S(2)–P(2)–C(9), 114.76(11); S(2)–P(2)–C(12), 122.46(11).

anti–syn π-plane, the relative orientation of two P-phenyl groups is alternated (alt) for **2N** and non-alternated (*non-alt*) for **8N** (Considering an anti–anti conformation as the standard π-plane, the observed orientations of two P-phenyl groups are defined as non-alt for **2N** and alt for **8N**). In spite of the different orientation of the P-phenyl groups, the structural features of the π-network observed for **2N** are similar to those observed for **8N**. In the crystal structure of Mathey's thiophene-linked π-system **K-1** (E = S) [6], one of the phosphole rings (syn conformation) is almost coplanar (3.3°) with the thiophene ring, whereas the other (anti conformation) significantly deviates from coplanarity (138.9°). The dissymmetry observed for *alt* **K-1** was attributed to packing effects in the crystalline state. In our pyrrole-linked π-systems **2N** and **8N**, the effective π-conjugation through the phosphole–pyrrole–phosphole linkage is exhibited as relatively small dihedral angles between the central pyrrole and adjacent syn/anti phosphole rings (9.9°/163.4° for **2N**, and 16.8°/175.8° for **8N**).

The C–C bond length alternation in the phosphole rings (Δl = 0.09–0.13 Å; Julg index = 0.55–0.73) in **2O, 2N**, and **8N** is obvious as compared to that of the central furan (Δl = 0.03–0.04 Å; Julg index = 0.95) and pyrrole (Δl = 0.01–0.02 Å; Julg index = 0.96–0.98), which reflects not only a marked difference in aromaticity between phosphole and the latter second-row heteroles but also effective conjugation through the heterole spacers. The interring C–C bond lengths of the P=S derivative **8N** [(1.422(4), 1.434(4) Å] are somewhat shorter than those reported for the thiophene-linked P=S derivative **K-1** [E = S; 1.452(4), 1.461(4) Å], which may indicate that the phosphole–pyrrole–phosphole π-conjugation is more effective than the phosphole–thiophene–phosphole π-conjugation.

Each phosphorus center forms a tetrahedral geometry with average C–P–C/C–P–O bond angles of 102.1°/116.2° for **2O** and 102.7°/115.7° for **2N**, and average C–P–C/C–P–S bond angles of 101.5°/116.4° for **8N**. The N–H group of the pyrrole ring is directed to the P-oxo (for **2N**) or P-thioxo group (for **8N**) of the syn phosphole unit. It seems likely that weak hydrogen-bonding interaction between the NH proton and the P-bound chalcogen atom is also present in the solid state [12].

Optical and Electrochemical Properties of 2,5-Bis(1,5-diphenylphosphol-2-yl)heteroles

To reveal intrinsic effects of the heterole spacers and the P-substituents on the optical and electrochemical properties of the present phosphole–heterole–phosphole π-systems, we measured UV–vis absorption and fluorescence spectra (Fig. 5), as well as the redox potentials of **1X** and **2X** in CH_2Cl_2. The results are summarized in Table 1 together with the data of **8N** and previously reported **1P**.

As shown in Fig. 5, the σ^3-P derivatives **1X** and the σ^4-P=O derivatives **2X** displayed intense absorption bands attributable to π–π^* transitions at around 460–500 nm and 490–520 nm, respectively. All of **1X** are moderately fluorescent, emitting orange fluorescence with quantum yields (Φ_f) of 0.03–0.26, whereas **2X** are weakly fluorescent ($\Phi_f < 0.01$). The spectral shapes of the pyrrole-linked derivatives **1N**/**2N** are slightly different from those of the furan-linked derivatives **1O**/**2O** and the thiophene-linked derivatives **1S**/**2S**, suggesting that the character of vibronic states of **1N**/**2N** is different from that of **1O**/**2O** and **1S**/**2S**. Both absorption and emission maxima (λ_{ab} and λ_{em}) vary appreciably depending on the heterole spacers, and the lowest π–π^* excitation energies for the σ^3-P and σ^4-P=O derivatives decrease in the orders, **1S** > **1O** > **1N** > **1P** and **2S** > **2O** > **2N**, respectively. As typically observed for π-conjugated phosphole derivatives, the oxidation at the phosphorus center from σ^3-P to σ^4-P=O induced redshifts of λ_{ab} and λ_{em} values, resulting in a decreased optical HOMO–LUMO gaps. The differences in $\lambda_{ab}/\lambda_{em}$ values ($\Delta\lambda_{ab}/\Delta\lambda_{em}$) between **1N** and **2N** (41/63 nm) are larger than those between **1X** and **2X** (**X** = **O**, 27/34 nm; **X** = **S**, 20/30 nm), indicating that the P-oxidation makes more significant impacts on the polarizability of the pyrrole-linked π-system than that of the furan- and thiophene-linked π-systems. Presumably, the charge-transfer character of the whole π-system is enhanced most effectively for the pyrrole-linked derivatives, as the highly electron-donating pyrrole ring and the highly electron-accepting P-oxo phosphole rings are connected in **2N**.

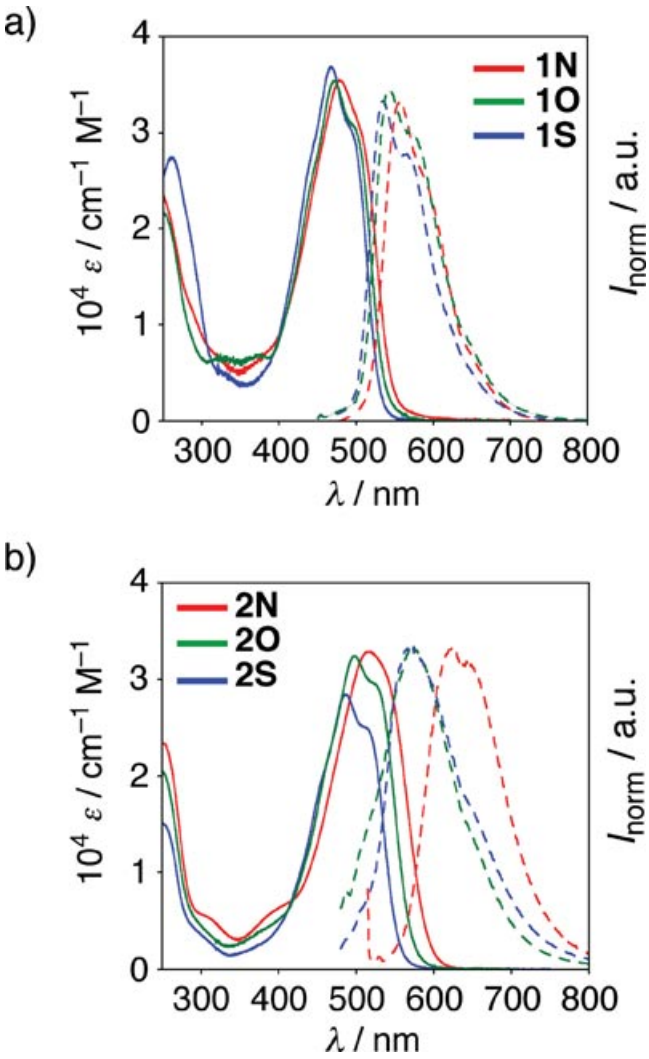

FIGURE 5 UV–vis absorption (solid line) and fluorescence (dashed line) spectra of **1X** and **2X** in CH_2Cl_2. The fluorescence spectra are normalized for comparison.

Redox potentials of **1X, 2X**, and **8N** (mixtures of diastereomers except for **2N**) were measured by using cyclic voltammetry (CV) and differential pulse voltammetry (DPV) with 0.1 M nBu$_4$NPF$_6$ as an electrolyte. Both electrochemical reduction and oxidation processes of the σ^4-P=O derivatives **2X** were observed at more positive potentials than those of the σ^3-P derivatives **1X**, indicating that the P-oxidation lowers HOMO and LUMO levels of the phosphole-heterole–phosphole π-systems. Compounds **1N, 1O**, and **1S** showed reversible voltammograms for the first oxidation process and irreversible voltammograms for the first reduction process. The first oxidation potentials (E_{ox}) of **1X** are shifted to the negative side in the order **1N** > **1O** ≈ **P** > **1S**, whereas the

TABLE 1 Optical and Electrochemical Data for **1X, 2X**, and **8N** in CH_2Cl_2

Compound	$\lambda_{ab}(nm)^a(\log \varepsilon)$	$\lambda_{em}(nm)^b(\Phi_f)$	$E_{ox}(V)^c$	$E_{red}(V)^c$	$E_g(V)^d$
1N[e]	478 (4.55)	561 (0.26)	+0.01 (*r*)	−2.36 (*ir*)	2.37
1O[e]	472 (4.55)	550 (0.03)	+0.16 (*r*)	−2.32 (*ir*)	2.48
1P[e,f]	502 (4.39)	634 (<0.01)	+0.16 (*ir*)	−2.10 (*ir*)	2.26
1S[e]	467 (4.57)	542 (0.05)	+0.24 (*r*)	−2.25 (*ir*)	2.49
2N[g]	519 (4.52)	624 (<0.01)	+0.32 (*ir*)	−1.90 (*qr*)	2.22
2O[e]	499 (4.51)	575 (<0.01)	+0.50 (*ir*)	−1.80 (*qr*)	2.30
2S[e]	487 (4.45)	572 (<0.01)	+0.57 (*ir*)	−1.78 (*qr*)	2.35
8N[g]	517 (4.49)	627 (<0.01)	+0.31 (*r*)	−1.90 (*ir*)	2.21

[a]The longest absorption maxima. Excited at 440 nm for **1X**; 470 nm for **2O** and **2S**; 510 nm for **2N** and **8N**.
[b]Fluorescence quantum yield relative to Réau's 3,4-C_4-bridged 1-phenyl-2,5-dithienylphosphole P–AuCl complex ($\Phi_f = 0.129$).
[c]The first oxidation (E_{ox}) and reduction (E_{red}) potentials (vs. Fc/Fc^+) determined by DPV. *r*: reversible; *qr*: quasi-reversible; *ir*: irreversible.
[d]$E_g = E_{ox} - E_{red}$.
[e]Mixture of diastereomers.
[f] Data from [9].
[g]Single diastereomer.

first reduction potentials (E_{red}) of **1X** are shifted to the positive side in the order, **1P** > **1S** > **1O** > **1N**. These orders are basically the same as the orders of ionization potential and electron affinity of pyrrole, furan, phosphole, and thiophene (at B3LYP/6-31G* level, HOMO/LUMO energies of pyrrole, furan, phosphole, and thiophene were calculated to be –5.48/+1.39, –6.11/+0.54, –6.25/–1.01, and –6.33/–0.21 eV, respectively) [13]. It is now evident that the electron-donating and electron-accepting ability of the phosphole–heterole–phosphole π-systems essentially reflects the character of the heterole spacers. For instance, the pyrrole-linked derivative **1N** possesses the highest electron-donating ability, whereas the phosphole-linked derivative **1P** has the highest electron-accepting ability. The electrochemical potential gaps ($E_g = E_{ox} - E_{red}$) decrease in the order, **1S** ≈ **O** > **1N** > **1P**. This trend is in good accordance with that observed in the absorption/emission spectra of **1X**. All the σ^4-P=O derivatives **2X** and **8N** displayed irreversible oxidation processes and quasi-reversible reduction processes in their cyclic voltammograms. Both E_{ox} and E_{red} of **2X** (as determined by DPV) shifted to more positive values in the order, **2S** > **2O** > **2N**, although the differences between **2S** and **2O** are small. Similar to a series of **1X**, this order correlates well with the ionization potentials and electron affinity of the respective heteroles incorporated. The P-functionalizations from σ^3 to σ^4 (**1X** to **2X/8N**) make more significant impacts on the reduction processes ($\Delta E_{red} = 0.46$–0.52 V) than the oxidation processes ($\Delta E_{ox} = 0.31$–0.34 V). As a result, the potential gaps of **2X/8N** ($E_g = 2.21$–2.35 V) become narrower than the respective values of **1X** ($E_g = 2.37$–2.49 V), which well explains the difference in the above-mentioned optical HOMO–LUMO gaps between **1X** and **2X/8N**.

Theoretical Calculations of 2,5-Bis(1-phenylphosphol-2-yl)heteroles

To get some insights into the intrinsic effects of the heterole spacers on the electronic structures of the present phosphole–heterole–phosphole π-systems, we performed density functional theory (DFT) calculations on model compounds **1Xm** (**X** = **N**, **O**, **P**, **S**) and **2Xm** (**X** = **N**, **O**, **S**). In this study, we calculated only non-alt diastereomers with anti–anti conformation for all the models (it was found that there is a negligible difference in total energy ($\Delta E =$ 1.4 kcal mol^{-1}) between alt and non-alt diastereomers of **2Om**). Selected torsion/bond angles, bond lengths and HOMO/LUMO energies are summarized in Table 2. At the optimized structures that have C_s symmetry, interring distortion between the central heterole ring and the adjacent anti phosphole rings are relatively small (C_3–C_2–$C_{2'}$–$C_{3'}$ torsion angle, $\alpha = 164.3$–169.8°), suggesting that the three heterole rings are effectively π-conjugated. The C_3–C_2–$C_{2'}$ bond angles (β) of **1Nm, 1Om**, and **2Om** are wider by 3.9–4.2° than those of **1Pm, 1Sm**, and **2Sm**, respectively, which simply reflects the different sizes between the second-row heteroles (pyrrole, furan) and the third-row heteroles (phosphole, thiophene). The P-oxidation (from **1Xm** to **2Xm**) induces coplanarization ($\Delta\alpha = 0.5$–2.9°) between the central heterole and the adjacent phosphole rings, namely enhancement of conjugation of the heterole-linked π-network. Indeed, the P-oxidation shortens the C–C bonds at *a* and *c* ($\Delta l = 0.002$–0.006 Å) and lengthens the C–C bonds at *b* ($\Delta l = 0.002$–0.004 Å). In other words, the bond length alternation is diminished by the P-oxidation. These effects are most prominent for the pyrrole-linked derivatives (from **1Nm** to **2Nm**), probably due to an increase in the

TABLE 2 Selected Torsion/Bond Angles, Bond Lengths, and Orbital Energies of **1Xm** and **2Xm**[a]

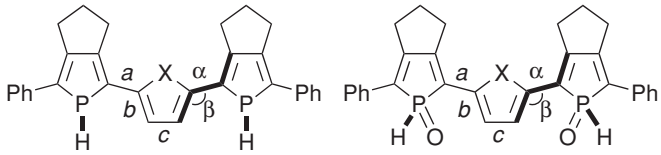

1Xm (*anti–anti*; *non-alt*) **2Xm** (*anti–anti*; *non-alt*)

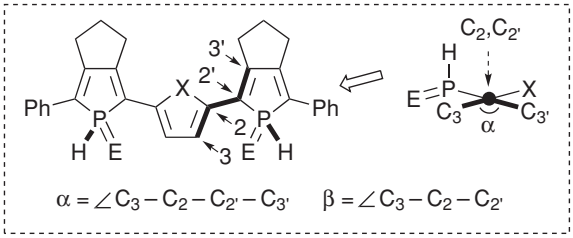

$\alpha = \angle C_3 - C_2 - C_{2'} - C_{3'}$ $\beta = \angle C_3 - C_2 - C_{2'}$

X	**1Nm** NH	**1Om** O	**1Pm** PH	**1Sm** S	**2Nm** NH	**2Om** O	**2Sm** S
α/°	164.3	169.3	169.4	165.9	167.2	169.8	166.8
β/°	130.2	132.0	126.1	128.1	129.2	131.1	126.9
a/Å	1.438	1.433	1.439	1.440	1.432	1.427	1.436
b/Å	1.399	1.381	1.378	1.386	1.403	1.383	1.389
c/Å	1.406	1.414	1.431	1.410	1.401	1.411	1.408
E_{LUMO}/eV	–1.77	–1.91	–2.11	–1.96	–2.43	–2.54	–2.54
E_{HOMO}/eV	–4.48	–4.60	–4.65	–4.69	–4.90	–5.03	–5.10

[a]Calculated at B3LYP/6–31G* level.

charge-transfer character of the pyrrole–phosphole linkage as compared to that of the furan–phosphole and thiophene–phosphole linkages. In the case of **2Nm**, a syn–anti form, which is the same as that observed for **2N** in the X-ray single-crystal structural analysis, was also calculated. The bond parameters of the π-conjugated units calculated for the syn–anti diastereomer (see Table 3) are close to those observed for **2N**. The difference in total energy between the two diastereomers of **2Nm** was found to be 5.2 kcal mol^{-1}, indicating that there is a small difference in their thermodynamic stability.

In both the σ^3-P models **1Xm** and the σ^4-P=O models **2Xm**, HOMO essentially consists of the conjugated polyene-derived π-networks, whereas LUMO possesses a significant character of the two phosphole subunits (Fig. 6). This is reasonable considering the intrinsic nature of the heterole spacers. As generally observed for the phosphole-containing π-systems, the P-oxidation (from **1Xm** to **2Xm**) lowers LUMO levels more significantly than HOMO levels due to the effective σ^*–π^* orbital interaction at the phosphole subunits. The heterole spacers play a crucial role in fine-tuning of the HOMO and LUMO

TABLE 3 Selected Torsion/Bond angles, Bond Lengths, and Orbital Energies of **2Nm** (syn-anti)[a]

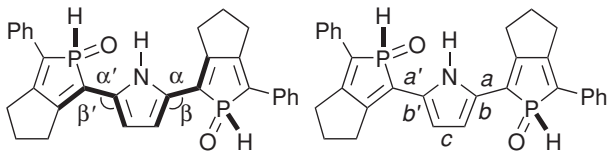

2Nm (*syn–anti*; *non-alt*)

α, α'/°	168.0, 18.2	*a*, *a*'/Å	1.434, 1.432	E_{LUMO}/eV	–2.35
β, β'/°	129.3, 133.4	*b*, *b*'/Å	1.406, 1.403	E_{HOMO}/eV	–4.82
		c/Å	1.402		

[a]Calculated at B3LYP/6–31G* level.

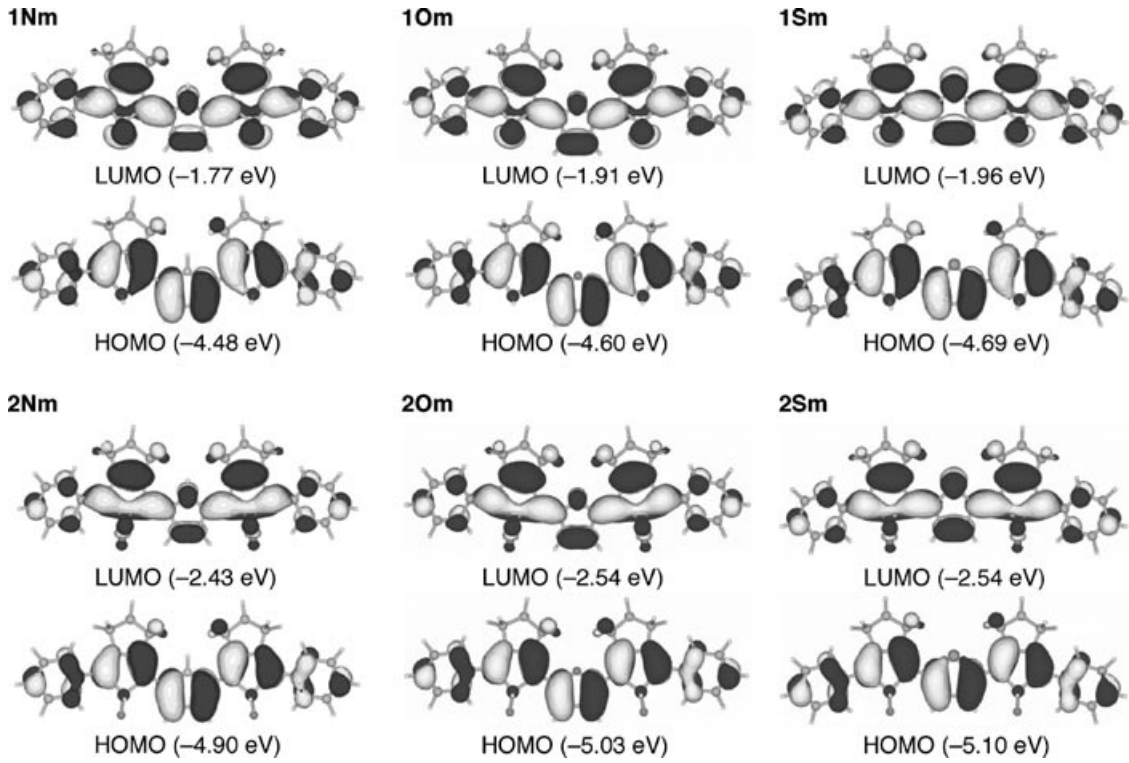

FIGURE 6 HOMO and LUMO of **1Xm** and **2Xm** and their orbital energies.

levels. The HOMO levels lower in the following orders: **1Nm** > **1Om** > **1Pm** > **1Sm** for the σ^3-P models and **2Nm** > **2Om** > **2Sm** for the σ^4-P=O models, whereas the LUMO levels lower in the following orders: **1Nm** > **1Om** > **1Sm** > **1Pm** for the σ^3-P models and **2Nm** > **2Om** ≈ **Sm** for the σ^4-P=O models. In both series, the pyrrole-linked models possess the highest HOMO and LUMO, whereas the thiophene- or phosphole-linked models possess the lowest ones. It is worth noting that these theoretical results mostly agree with the experimental results of the redox potentials determined by CV and DPV.

CONCLUSION

In summary, we established a convenient method for the synthesis of 2,5-bis(1,5-diphenylphosphol-2-yl)heterole derivatives and investigated their structural, optical, and electrochemical properties comparatively. It has been revealed for the first time that the fundamental properties of the phosphole–heterole–phosphole π-systems, in both σ^3-P and σ^4-P=O forms, are deeply related to the intrinsic nature of the central heterole spacers. Most importantly, the present results provide a practical guideline to fine-tune the character of HOMO and LUMO of the phosphole–based π-conjugated materials, especially those containing phosphole–heterole linkages, on the basis of rational design of the π-components.

EXPERIMENTAL

All melting points were recorded on a Yanagimoto micro melting point apparatus and are uncorrected. ^{1}H, ^{13}C, and ^{31}P NMR spectra were recorded on a JEOL JNM-EX400 spectrometer using $CDCl_3$, CD_2Cl_2, or $Cl_2CDCDCl_2$. Chemical shifts are reported in ppm as relative values versus tetramethylsilane (internal reference for ^{1}H and ^{13}C) and phosphoric acid (external reference for ^{31}P). High-resolution mass spectra (HRMS) were obtained on a JEOL JMS-HS110 spectrometer or a Thermo Scientific Exactive Spectrometer. IR spectra were recorded on a JASCO FT/IR-470 Plus spectrometer using KBr pellets. UV–vis absorption spectra were measured on a PerkinElmer Lambda 900 UV/vis/NIR spectrometer. Steady-state fluorescence spectra were recorded with a HORIBA SPEX Fluoromax-3 spectrofluorometer. Electrochemical measurements were made with an ALS 630a electrochemical analyzer using a glassy carbon working electrode, a platinum wire counter electrode, and an Ag/Ag^+ [0.01 M $AgNO_3$, 0.1 M nBu$_4$NPF$_6$

(MeCN)] reference electrode. The potentials were calibrated with ferrocene/ferrocenium [$E_{mid} = +0.20$ V vs. Ag/Ag^+]. Phospholes **3** and **4** were prepared according to the reported procedures [10]. The solvents used for the reactions were distilled from sodium benzophenone ketyl (THF and Et_2O) or calcium hydride (CH_2Cl_2) under inert atmosphere before use. Other chemicals and solvents were of reagent-grade quality and used without further purification. All reactions were performed under an argon atmosphere.

Compound **2O**

$Pd_2(dba)_3$ (9.2 mg, 0.010 mmol) and tris(2-furyl)phosphane (9.2 mg, 0.040 mmol) were stirred in NMP (1.0 mL) for 1 h at room temperature. To this mixture, an NMP solution (1.5 mL) containing **4** (88.1 mg, 0.21 mmol) and 2,5-bis(tributylstannyl)furan (64.6 mg, 0.10 mmol) was added. The mixture was stirred for 47 h at 80°C, followed by addition of a saturated aqueous NH_4Cl solution. The aqueous phase was extracted with EtOAc three times, and an organic phase was washed with brine, dried over Na_2SO_4, and evaporated under reduced pressure. The residue was subjected to silica gel column chromatography ($CHCl_3$ to $CHCl_3$/acetone/MeOH = 70/10/1), and a red fraction was collected and evaporated. Reprecipitation of the resulting solid from $CHCl_3$/hexane afforded **2O** as a purplish red solid (17.5 mg, 27%; a mixture of the two diastereomers). Diastereomers were separated by silica gel column chromatography ($CHCl_3$/acetone = 10/1 to 8/1).

2O-A: Brownish red solid; mp 250°C (dec); ^{1}H NMR (400 MHz, $CDCl_3$): δ 2.12–2.23 (m, 2H; CH_2), 2.31–2.38 (m, 2H; CH_2), 2.86–3.01 (m, 6H; CH_2), 3.15–3.20 (m, 2H; CH_2), 6.47 (s, 2H; furan-β), 7.20 (t, J = 7.4 Hz, 2H; *p*-Ph), 7.29 (t, J = 7.4 Hz, 4H; *m*-Ph), 7.37 (dt, J = 2.4, 7.0 Hz, 4H; *m*-Ph–P), 7.45 (t, J = 7.2 Hz, 2H; *p*-Ph–P), 7.61 (d, J = 7.6 Hz, 4H; *o*-Ph), 7.76 ppm (dd, J = 7.2, 12.0 Hz, 4H; *o*-Ph–P); ^{13}C NMR (100 MHz, $CDCl_3$): δ 26.4, 29.7 (d, J = 10.7 Hz), 30.1 (d, J = 12.3 Hz), 113.4, 117.4 (d, J = 101.6 Hz), 126.1 (d, J = 100.8 Hz), 127.6 (d, J = 7.4 Hz), 127.7, 128.8, 128.9 (d, J = 12.3 Hz), 130.3 (d, J = 91.7 Hz), 130.4 (d, J = 10.7 Hz), 132.1 (d, J = 2.5 Hz), 133.1 (d, J = 13.3 Hz), 149.5 (d, J = 24.0 Hz), 152.4 (d, J = 23.1 Hz), 155.8 (d, J = 24.8 Hz); ^{31}P NMR (162 MHz, $CDCl_3$): δ +52.5; IR(KBr); ν_{max} 1195 cm^{-1} (P=O).

2O-B: Red solid; mp 252°C (dec); ^{1}H NMR (400 MHz, $CDCl_3$): δ 2.11–2.18 (m, 2H; CH_2), 2.28–2.38 (m, 2H; CH_2), 2.83–2.97 (m, 8H, CH_2), 6.49 (s, 2H; furan-β), 7.20 (t, J = 7.6 Hz, 2H; *p*-Ph), 7.29 (t, J = 7.6 Hz, 4H; *m*-Ph), 7.36–7.40 (m, 4H; *m*-Ph–P), 7.43–7.47 (*m*, 2H; *p*-Ph–P), 7.60 (d, J = 7.6 Hz, 4H; *o*-Ph), 7.76–7.81 (m, 4H; *o*-Ph–P); ^{13}C NMR (100 MHz, $CDCl_3$): δ 26.4, 29.6 (d, J = 9.9 Hz), 30.1 (d, J = 12.4 Hz), 113.1 (d, J = 2.5 Hz), 117.2 (d, J = 101.7 Hz), 126.0 (d, J = 100.0 Hz), 127.6 (d, J = 6.6 Hz), 127.7, 128.8, 128.9 (d, J = 11.6 Hz), 130.3 (d, J = 91.7 Hz), 130.5 (d, J = 10.7 Hz), 132.1 (d, J = 2.5 Hz), 133.1 (d, J = 9.9 Hz), 149.4 (d, J = 21.5 Hz), 153.2 (d, J = 23.1 Hz), 155.8 (d, J = 24.8 Hz); ^{31}P NMR (162 MHz, $CDCl_3$): δ +52.7; IR(KBr): ν_{max} 1193 cm^{-1} (P=O); HRMS (APCI) *m/z*: Calcd for $C_{42}H_{35}O_3P_2$: 649.2061; Found 649.2048 ($[M + H]^+$).

Compound **1O**

A mixture of **2O** (64.6 mg, 0.10 mmol), $HSiCl_3$ (0.50 mL, 4.9 mmol), and $CHCl_3$ (5.0 mL) was stirred at 80°C. After 2 h the mixture was concentrated under reduced pressure to remove unreacted $HSiCl_3$, followed by addition of a saturated aqueous $NaHCO_3$ solution. Insoluble substances were filtered off through a Celite bed, and the organic phase was washed with water, dried over Na_2SO_4, and evaporated under reduced pressure. Reprecipitation of the resulting solid from CH_2Cl_2/MeOH afforded **1O** as a reddish orange solid (45.1 mg, 74%).

1O: mp (a mixture of 1:1 diastereomers) 215°C (dec); ^{1}H NMR (400 MHz, $CDCl_3$): δ 2.32–2.40 (m, 4H; CH_2), 2.55–3.02 (m, 8H; CH_2), 6.18 (s, 2H; furan-β; isomer **A**), 6.21 (s, 2H; furan-β; isomer **B**), 7.08–7.13 (m, 2H; *p*-Ph), 7.20–7.25 (*m*, 10H; *m*-Ph + *m*-Ph–P + *p*-Ph–P), 7.43–7.47 (m, 8H; *o*-Ph + *o*-Ph–P); ^{31}P NMR (162 MHz, $CDCl_3$): δ +30.6, +31.0; HRMS (APCI) *m/z*: Calcd for $C_{42}H_{34}OP_2$: 616.2085; Found 616.2077 (M^+).

Compound **2S**

$Pd_2(dba)_3$ (13.5 mg, 0.015 mmol) and tris(2-furyl)phosphane (13.6 mg, 0.059 mmol) were stirred in NMP (1.5 mL) for 1 h at room temperature. To this mixture, an NMP solution (6.0 mL) containing **3** (368.7 mg, 0.63 mmol) and 2,5-diiodothiophene (98.9 mg, 0.29 mmol) was added. After Ar bubbling for 30 min, CuI (127.2 mg, 0.68 mmol) was added and the resulting mixture was stirred for 1.5 h at the room temperature. Cold EtOAc (24 mL) was added to the mixture, and brown precipitates were collected. The crude product was dissolved in $CHCl_3$, and insoluble substances were filtered off through a Celite bed. The red solution was evaporated and reprecipitated from $CHCl_3$/hexane to give analytically pure **2S** as a reddish orange solid (148 mg, 75%).

because of the low solubility, we did not attempt to separate two diastereomers of **2S**. mp (a mixture of 6:4 diastereomers) 200°C (dec); ^{1}H NMR ($CDCl_3$, 400 MHz): δ 2.11–2.22 (m, 2H; CH_2), 2.31–2.40 (m, 2H; CH_2), 2.75–3.03 (m, 8H; CH_2), 7.16 (s, 2H; Th-β; isomer **A**), 7.19 (s, 2H; Th-β; isomer **B**), 7.19 (t, J = 7.3 Hz, 2H; *p*-Ph), 7.29 (pseudo t, J = 7.8 Hz, 4H; *m*-Ph), 7.33–7.39 (m, 4H; *m*-Ph–P), 7.40–7.46 (m, 2H; *p*-Ph–P), 7.61 (d, J = 7.3 Hz. 4H; *o*-Ph), 7.74–7.79 (m, 4H; *o*-Ph–P); ^{31}P{^{1}H} NMR ($CDCl_3$, 162 MHz): δ +52.8, 53.1; IR (KBr): ν_{max} 1181 (P= O) cm^{-1}; HRMS (APCI) *m*/*z*: Calcd for $C_{42}H_{35}O_2P_2S$: 665.1833; Found 665.1812 ([M + H]$^+$).

Compound **1S**

A mixture of **2S** (68.1 mg, 0.10 mmol), $HSiCl_3$ (0.20 mL, 2.0 mmol), and $CHCl_3$ (35 mL) was stirred for 20 h at 70°C. After adding additional $HSiCl_3$ (0.40 mL, 4.0 mmol), the resulting mixture was stirred further for 77 h at 80°C. A saturated aqueous NH_4Cl solution was added to the mixture, and insoluble substances were filtered off through a Celite bed. The aqueous layer was extracted with $CHCl_3$, and the organic phase was washed with brine, dried over Na_2SO_4, and evaporated under reduced pressure. The residue was subjected to short silica gel column chromatography ($CHCl_3$), and the orange fraction was collected, evaporated, and reprecipitated from $CHCl_3$/MeOH to give **1S** as an orange solid (28.4 mg, 44%). mp (a mixture of 1:1 diastereomers) 265°C (dec); ^{1}H NMR ($Cl_2CDCDCl_2$, 400 MHz): δ 2.31–2.39 (m, 4H; CH_2), 2.68–3.01 (m, 8H; CH_2), 6.76 (s, 2H; Th-β; isomer **A**), 6.77 (s, 2H; Th-β; isomer **B**), 7.10 (t, J = 7.2 Hz, 2H; *p*-Ph), 7.19–7.25 (m, 10H; *m*-Ph + *m*-Ph–P + *p*-Ph–P), 7.41 (d, J = 7.2 Hz, 4H; *o*–Ph), 7.43–7.45 (m, 4H; *o*-Ph–P); ^{31}P{^{1}H} NMR ($CDCl_3$, 162 MHz): δ +33.5, +33.7; IR (KBr): HRMS (EI) *m*/*z*: Calcd for $C_{42}H_{35}P_2S$: 633.1935; Found 633.1913 ([M + H]$^+$).

Compound **7N**

$Pd_2(dba)_3$ (422 mg, 0.461 mmol) and tris(2-furyl)phosphane (214 mg, 0.922 mmol) were stirred in NMP (30 mL) for 2 h at room temperature. An NMP solution (30 mL) containing **5** (2.95 g, 5.07 mmol), **6** (966 mg, 2.31 mmol), and CuI (878 mg, 4.61 mmol) was added, and the resulting mixture was stirred for 1 h at the same temperature. The mixture was then added into a mixture of AcOEt and aq. NH_4Cl, and the organic phase was separated, washed with aq NH_4Cl and brine, and dried over Na_2SO_4. After removal of solvents under reduced pressure, the resulting mixture was subjected to silica gel column chromatography (CH_2Cl_2 to CH_2Cl_2/acetone = 1/1) to give **7N-A** (R_f = 0.45 CH_2Cl/acetone = 10/1) and **7N-B** (R_f = 0.20 at CH_2Cl/acetone = 10/1). After reprecipitation from hexane, **7N-B** was obtained as an orange solid (339 mg, 20%). By contrast, **7N-A** (ca. 550 mg, ca. 33%) was obtained as a mixture with a small amount of the side product, 2,2'-biphosphole [10].

7N-A. Red solid; ^{1}H NMR ($CDCl_3$, 400 MHz): δ 1.45 (s, 9H; Boc), 1.99–2.09 (m, 2H; CH_2), 2.20–2.28 (m, 2H: CH_2), 2.62–2.72 (m, 4H; CH_2), 2.90–3.00 (m, 4H; CH_2), 6.03 (s, 2H; pyrrole-β), 7.20 (t, J = 7.3 Hz, 2H; *p*-Ph), 7.29 (pseudo t, J = 7.6 Hz, 4H; *m*-Ph), 7.34–7.38 (m, 4H; *m*-Ph–P), 7.43–7.46 (m, 2H; *p*-Ph–P), 7.61 (d, J = 7.8 Hz, 4H; *o*-Ph), 7.76 ppm (dd, J = 7.3, 12.2 Hz, 4H; *o*-Ph–P); ^{31}P{^{1}H} NMR ($CDCl_3$, 162 MHz): δ +52.8. As the biphosphole could not be removed completely, only ^{1}H and ^{31}P NMR data are reported herewith.

7N-B. Orange solid; mp 154–155°C (dec); ^{1}H NMR ($CDCl_3$, 400 MHz): δ 1.36 (s, 9H; Boc), 1.87–1.97 (m, 2H; CH_2), 2.23–2.30 (m, 2H; CH_2), 2.61–3.01 (m, 8H; CH_2), 6.44 (s, 2H; pyrrole-β), 7.21 (t, J = 7.3 Hz, 2H; *p*-Ph), 7.26–7.37 (m, 8H; *m*-Ph + *m*-Ph–P), 7.39 (t, J = 6.8 Hz, 2H; *p*-Ph–P), 7.69 (d, J = 7.3 Hz, 4H; *o*-Ph), 7.70–7.75 (m, 4H; *o*-Ph–P); ^{31}P{^{1}H} NMR ($CDCl_3$, 162 MHz): δ +51.9; IR (KBr): ν = 1193 (P=O), 1746 (C=O) cm^{-1}; UV–vis (CH_2Cl_2): λ_{max} (log ε) 448 nm (4.29); HRMS (FAB) *m*/*z*: Calcd for $C_{47}H_{44}NO_4P_2$: 748.2746; Found 748.2746 ([M +H]$^+$).

Synthesis of **8N**

To a toluene solution (1 mL) of **7N-A** (21 mg, ca. 0.028 mmol), Lawesson's reagent (11.4 mg, 0.0282 mmol) was added at room temperature. After stirring for 3 h under reflux, CH_2Cl_2 and aq. $NaHCO_3$ were added into the reaction mixture. The aqueous phase was extracted with CH_2Cl_2, and the combined organic extracts were dried over Na_2SO_4. After removal of solvents under reduced pressure, the resulting mixture was subjected to alumina column chromatography (CH_2Cl_2). The reddish-purple fraction was collected, evaporated and reprecipitated from CH_2Cl_2/hexane to give **8N-A** (8.0 mg, 42%). According to a similar procedure, **8N-B** was prepared in 82% yield from **7N-B**.

8N-A. Red solid; Mp 180°C (dec); ^{1}H NMR (CD_2Cl_2, 400 MHz): δ 2.24–2.47 (m, 4H), 2.76–3.03 (m, 8H), 6.36 (s, 2H, pyrrole-β), 7.18–7.21 (m, 2H), 7.26–7.30 (m, 4H), 7.31–7.46 (m, 6H), 7.51–7.57 (m, 4H), 7.96–8.01 (m, 4H, *o*-Ph-P), 10.20 (s, 1H, NH); ^{13}C{^{1}H} NMR ($CDCl_3$, 75 MHz): δ 25.8, 27.6 (d, J = 11.2 Hz), 28.8 (d, J = 11.2 Hz), 110.9 (d,

J = 7.4 Hz), 120.2 (d, J = 83.7 Hz), 123.8 (d, J = 60.4 Hz), 125.8 (d, J = 7.4 Hz), 125.8, 126.3 (d, J = 14.9 Hz), 126.9 (d, J = 70.1 Hz), 127.0, 127.4 (d, J = 11.8 Hz), 129.0 (d, J = 11.8 Hz), 156. 2 (d, J = 22.3 Hz); $^{31}P\{^1H\}$ NMR (CD_2Cl_2, 162 MHz) δ +64.5; HRMS (FAB) m/z: Calcd for $C_{42}H_{35}NP_2S_2$: 679.1686; Found 679.1666 (M^+). Anal. Calcd for $C_{42}H_{35}NP_2S_2$: C, 74.20; H, 5.19; N 1.97. Found: C, 73.98; H, 5.49; N, 2.06%.

8N-B. Brown solid. mp 205°C (dec); ^1H NMR ($CDCl_3$, 400 MHz): δ 2.25–2.40 (m, 4H), 2.74–3.00 (m, 8H), 6.39 (d, J = 2.4 Hz, 2H, pyrrole-β), 7.15–7.20 (m, 2H), 7.24–7.28 (m, 4H), 7.35–7.47 (m, 6H), 7.55–7.58 (m, 4H), 7.85–7.91 (m, 4H, o-Ph–P), 10.24 (s, 1H, NH); $^{31}P\{^1H\}$ NMR (CD_2Cl_2, 162 MHz) δ +65.9.

Compound **1N**

A toluene solution (5 mL) containing **8N-A** (112 mg, 0.164 mmol) and $P(NMe_2)_3$ (0.30 mL, 1.6 mmol) was heated at reflux for 1 h. The reaction mixture was concentrated under reduced pressure, and a solid residue was subjected to silica gel column chromatography (hexane/CH_2Cl_2 = 5/1). The orange fraction (R_f = 0.2) was collected, evaporated, and reprecipitated from CH_2Cl_2/hexane to give **1N-A** as a brownish red solid (84 mg, 83%). mp (a mixture of two diastereomers) 213–214°C; ^1H NMR (CD_2Cl_2, 400 MHz): δ 2.32–2.77 (m, 10H; CH_2), 2.94–3.03 (m, 2H; CH_2), 6.16 (d, J = 2.4 Hz, 2H, pyrrole-β, isomer **A**), 6.20 (d, J = 2.4 Hz, 2H, pyrrole-β, isomer **B**), 7.10 (t, J = 7.3 Hz, 2H; p-Ph), 7.23–7.33 (m, 10H; m-Ph + m-Ph–P + p-Ph–P), 7.42–7.50 (m, 8H; o-Ph + o-Ph–P), 7.96 (s, 1H; NH, isomer **A**), 8.04 ppm (s, 1H; NH, isomer **B**); $^{31}P\{^1H\}$ NMR ($CDCl_3$, 162 MHz) δ +29.3, +29.6; HRMS (EI) m/z: Calcd for $C_{42}H_{35}NP_2$: 615.2245; Found: 615.2262 (M^+).

Compound **2N**

A solid of **7N** (one of the diastereomers; 32.2 mg, 0.044 mmol) was heated at 180°C without solvent under argon atmosphere. After 30 min, a solid residue was subjected to silica gel column chromatography (CH_2Cl_2 to CH_2Cl_2/acetone = 10/3) and a red fraction was collected and evaporated under reduced pressure. Recrystallization of the resulting solid from CH_2Cl_2/hexane gave **2N** as a brown solid (23.1 mg, 81%). mp (single diastereomer) 284–285°C (dec); ^1H NMR (CD_2Cl_2, 300 MHz): δ 2.11–2.18 (m, 2H; CH_2), 2.36–2.41 (m, 2H; CH_2), 2.78–3.00 (m, 8H; CH_2), 6.41 (d, J = 2.6 Hz, 2H; pyrrole-β), 7.20 (t, J = 7.3 Hz, 2H; p-Ph), 7.29–7.38 (m, 8H; m-Ph + m-Ph–P), 7.42–7.48 (m, 2H; p-Ph–P), 7.62 (d, J = 8.1 Hz, 4H; o-Ph), 7.71–7.78 (m, 4H; o-Ph–P), 9.75 (s, 1H; NH); $^{13}C\{^1H\}$ NMR ($CDCl_3$, 100 MHz): δ 26.3, 28.9 (d, J = 10.7 Hz), 30.2 (d, J = 12.3 Hz), 112.7 (d, J = 5.0 Hz), 119.0 (d, J = 99.2 Hz), 127.4, 127.4 (d, J = 3.3 Hz), 128.5 (d, J = 15.8 Hz), 128.8, 129.0 (d, J = 12.3 H), 130.4 (d, J = 10.7 Hz), 130.5 (d, J = 90.1 Hz), 132.0, 133.3 (d, J = 14.1 Hz), 148.8 (d, J = 24.8 Hz), 156.6 (d, J = 26.5 Hz). One of the ^{13}C NMR peak (*ipso*-Ph) could not be detected clearly; $^{31}P\{^1H\}$ NMR ($CDCl_3$, 162 MHz) δ +54.2; HRMS (EI) m/z: Calcd for $C_{42}H_{35}NP_2$: 648.2221; Found 648.2208 ($[M + H]^+$).

X-ray Crystal Structure Analysis

Single crystals of **2O**, **2N**, and **8N** were grown from CH_2Cl_2–MeOH. All measurements were made on a Rigaku Mercury-8 CCD area detector with graphite monochromated Mo Kα radiation at 143 K. The structures were solved by a direct method (SIR92) [14] and expanded using Fourier techniques [15]. Non-hydrogen atoms were refined anisotropically, and hydrogen atoms were refined using the rigid model. All calculations were performed using CrystalStructure [16] crystallographic software package except for refinement, which was performed using SHELXL-97 [17]. Crystal data and structural refinement parameters are as follows. **2O**: $C_{42}H_{34}O_3P_2$, red plate, 0.30 × 0.20 × 0.05 mm, MW = 733.565, monoclinic, space group = $P2_1/n$, a = 12.341(9) Å, b = 18.503(14) Å, c = 16.000(12) Å, β = 95.581(13)°, V = 3636(5) Å^3, Z = 4, D_c = 1.340 g cm^{-3}, μ = 3.07 cm^{-1}, 27,060 obsd, 8181 unique, 452 variables, R_w = 0.2153, R = 0.0945 ($I > 2.0\ \sigma(I)$), GOF = 1.037. **2N**: $C_{42}H_{35}NO_2P_2$, red plate, 0.30 × 0.20 × 0.02 mm, MW = 647.69, monoclinic, space group = $P2_1/c$, a = 17.242(9) Å, b = 8.028(4) Å, c = 26.568(15) Å, β = 108.435(6)°, V = 3489(3) Å^3, Z = 4, D_c = 1.233 g cm^{-3}, μ = 1.615 cm^{-1}, 25,224 obsd, 7732 unique, 425 variables, R_w = 0.1857, R = 0.0804 ($I > 2.0\sigma(I)$), GOF = 1.180. **8N**: $C_{42}H_{35}NP_2S_2$, red plate, 0.40 × 0.20 × 0.08 mm, MW = 679.77, monoclinic, space group = $P2_1/n$, a = 12.908(4) Å, b = 18.863(5) Å, c = 13.944(4) Å, β = 91.488(4)°, V = 3394.1(16) Å^3, Z = 4, D_c = 1.330 g cm^{-3}, μ = 2.84 cm^{-1}, 38,747 obsd, 7547 unique, 425 variables, R_w = 0.1538, R = 0.0834 ($I > 2.0\sigma(I)$), GOF = 1.300. CCDC-788678, CCDC-788679, and CCDC-788680 contain the supplementary crystallographic data for **2O, 2N**, and **8N**, respectively. These data can be obtained free of charge via www.ccdc.cam.ac.uk/conts/retrieving.html (or from the Cambridge Crystallographic Data Centre, 12,

Union Road, Cambridge CB2 1EZ, UK; fax: +44 1223 336033; or deposit@ccdc.cam.ac.uk).

Computational Details

The geometry optimization was performed by the B3LYP method [18] with basis sets of 6-31G* [19]. We carried out vibration analysis with the B3LYP method to ascertain that each optimized geometry was not in saddle, but in equilibrium points. All calculations were carried out with the Gaussian 03 package [20]. The definitions of torsion angle α and bond angle β are shown in Table 3.

REFERENCES

[1] For recent reviews on π-conjugated phospholes, see: (a) Mathey, F. Angew Chem, Int Ed 2003, 42, 1578; (b) Hissler, M.; Dyer, P. W.; Réau, R. Top Curr Chem 2005, 250, 127; (c) Hissler, M.; Dyer, P. W.; Réau, R. Coord Chem Rev 2003, 244, 1; (d) Baumgartner, T.; Réau, R. Chem Rev 2006, 106, 4681; Correction: 2007, 107, 303; (e) Hissler, M.; Lescop, C.; Réau, R. Pure Appl Chem 2007, 79, 201; (f) Hobbs, M. G.; Baumgartner, T. Eur J Inorg Chem 2007, 3611; (g) Réau, R.; Dyer, P. W. In Comprehensive Heterocyclic Chemistry III; Ramsden, C. A.; Scriven, E. F. V.; Taylor, R. J. K. (Eds.); Elsevier: Oxford, UK, 2008; Ch. 3.15, pp. 1029–1048; (h) Hissler, M.; Lescop, C.; Réau, R. C R Chim 2008, 11, 628; (i) Matano, Y.; Imahori, H. Org Biomol Chem 2009, 7, 1258; (j) Fukazawa, A.; Yamaguchi, S. Chem Asian J 2009, 4, 1386.

[2] 2-Thienyl: (a) Hay, C.; Fischmeister, C.; Hissler, M.; Toupet, L.; Réau, R. Angew Chem, Int Ed 2000, 39, 1812; (b) Hay, C.; Hissler, M.; Fischmeister, C.; Rault-Berthelot, J.; Toupet, L.; Nyulászi, L.; Réau, R. Chem Eur J 2001, 7, 4222; (c) Fave, C.; Cho, T. -Y.; Hissler, M.; Chen, C. -W.; Luh, T. -Y.; Wu, C. -C.; Réau, R. J Am Chem Soc 2003, 125, 9254; (d) Fave, C.; Hissler, M.; Kárpáti, T.; Rault-Berthelot, J.; Deborde, V.; Toupet, L.; Nyulászi, L.; Réau, R. J Am Chem Soc 2004, 126, 6058; (e) Su, H. -C.; Fadhel, O.; Yang, C. -J.; Cho, T. -Y.; Fave, C.; Hissler, M.; Wu, C. -C.; Réau, R. J Am Chem Soc 2006, 128, 983; (f) Casado, J.; Réau, R.; López Navarrete, J. T. Chem Eur J 2006, 12, 3759; (g) Miyajima, T.; Matano, Y.; Imahori, H. Eur J Org Chem 2008, 255; (h) Matano, Y.; Miyajima, T.; Fukushima, T.; Kaji, H.; Kimura, Y.; Imahori, H. Chem Eur J 2008, 14, 8102; (i) Fadhel, O.; Gras, M.; Lemaitre, N.; Deborde, V.; Hissler, M.; Geffroy, B.; Réau, R. Adv Mater 2009, 21, 1261; (j) Fadhel, O.; Szieberth, D.; Deborde, V.; Lescop, C.; Nyulászi, L.; Hissler, M.; Réau, R. Chem Eur J 2009, 15, 4914.

[3] 2-Thienyl/2-phospholyl: (a) Bevierre, M. -O.; Mercier, F.; Ricard, L.; Mathey, F. Angew Chem, Int Ed Engl 1990, 29, 655; (b) Bevierre, M. -O.; Mercier, F.; Mathey, F.; Justand, A.; Amatore, C. New J Chem 1991, 15, 545.

[4] 2-Phospholyl: Deschamps, E.; Ricard, L.; Mathey, F. Angew Chem, Int Ed Engl 1994, 33, 1158.

[5] 2-Pyrrolyl: Matano, Y.; Fujita, M.; Saito, A.; Imahori, H. C R Chim 2010, 13, 1035.

[6] Deschamps, E.; Ricard, L.; Mathey, F. Heteroatom Chem 1991, 2, 377.

[7] (a) Hay, C.; Sauthier, M.; Deborde, V.; Hissler, M.; Toupet, L.; Réau, R. J Organomet Chem 2002, 643–644, 494; (b) Hay, C.; Fave, C.; Hissler, M.; Rault-Berthelot, J.; Réau, R. Org Lett 2003, 5, 3467.

[8] (a) Sebastian, M.; Hissler, M.; Fave, C.; Rault-Berthelot, J.; Odin, C.; Réau, R. Angew Chem, Int Ed 2006, 45, 6152; (b) Carrasco, P. M.; Pozo-Gonzalo, C.; Grande, H.; Pomposo, J. A.; Cortázar, M.; Deborde, V.; Hissler, M.; Réau, R. Polym Bull 2008, 61, 713; (c) de Talancé, V. L.; Hissler, M.; Zhang, L. -Z.; Kárpáti, T.; Nyulászi, L.; Caras-Quintero, D.; Bäuerle, P.; Réau, R. Chem Commun 2008, 2200.

[9] Matano, Y.; Nakashima, M.; Imahori, H. Angew Chem, Int Ed 2009, 48, 4002.

[10] Saito, A.; Matano, Y.; Imahori, H. Org Lett 2010, 12, 2675.

[11] For example, see: (a) Egan, W.; Tang, R.; Zon, G.; Mislow, K. J Am Chem Soc 1970, 92, 1442; (b) Egan, W.; Tang, R.; Zon, G.; Mislow, K. J Am Chem Soc 1971, 93, 6205; (c) Pelzer, S.; Wichmann, K.; Wesendrup, R.; Schwerdtfeger, P. J Phys Chem A 2002, 106, 6387.

[12] Bernstein, J.; Davis, R. E.; Shimoni, L.; Chang, N. -L. Angew Chem, Int Ed Engl 1995, 34, 1555.

[13] For example, see: (a) Kunii, T. L.; Kuroda, H. Theoret Chim Acta (Berlin) 1968, 11, 97; (b) von Niessen, W.; Cederbaum, L. S.; Diercksen, G. H. F. J Am Chem Soc 1976, 98, 2066; (c) Brédas, J. L.; Silbey, R.; Boudreaux, D. S.; Chance, R. R. J Am Chem Soc 1983, 105, 6555; (d) Kishimoto, N.; Yamakado, H.; Ohno, K. J Phys Chem 1996, 100, 8204; (e) De Proft, F.; Sablon, N.; Tozer, D. J.; Geerlings, P. Faraday Discuss 2007, 135, 151.

[14] Altomare, A.; Cascarano, G.; Giacovazzo, C.; Guagliardi, A.; Burla, M.; Polidori, G.; Camalli, M. J Appl Cryst 1994, 27, 435.

[15] Beurskens, P. T.; Admiraal, G.; Beurskens, G.; Bosman, W. P.; deGelder, R.; Israel, R.; Smits, J. M. M. The DIRDIF program system, Technical Report of the Crystallography Laboratory, University of Nijmegen, The Netherlands; 1999.

[16] Crystal Structure 3.8.2: CrystalStructure Analysis Package, Rigaku and Rigaku/MSC (2000–2006). 9009 New Trails Dr. The Woodlands TX 77381, USA.

[17] Sheldrick, G. M. University of Göttingen, Göttingen, Germany, 1997.

[18] (a) Becke, A. D. J Chem Phys 1988, 98, 5648; (b) Lee, C.; Yang, W.; Parr, R. G. Phys Rev B 1988, 37, 785.

[19] (a) Hehre, W. J.; Ditchfield, R.; Pople, J. A. J Chem Phys 1972, 56, 2257; (b) Francl, M. M.; Pietro, W. J.; Hehre, W. J.; Binkley, J. S.; DeFrees, D. J.; Pople, J. A.; Gordon, M. S. J Chem Phys 1982, 77, 3654; (c) Clark, T.; Chandrasekhar, J.; Spitznagel, G. W.; Schleyer, P. von R. J Comp Chem 1983, 4, 294.

[20] Gaussian 03, Revision C.02; Gaussian, Inc.: Wallingford CT, 2004 Frisch, M. J.; Trucks, G. W.; Schlegel, H. B.; Scuseria, G. E.; Robb, M. A.; Cheeseman, J. R.; Montgomery, J. A., Jr.; Vreven, T.; Kudin, K. N.; Burant, J. C.; Millam, J. M.; Iyengar, S. S.; Tomasi, J.; Barone, V.; Mennucci, B.; Cossi, M.; Scalmani, G.; Rega, N.; Petersson, G. A.; Nakatsuji, H.; Hada, M.; Ehara, M.; Toyota, K.; Fukuda, R.; Hasegawa, J.;

Ishida, M.; Nakajima, T.; Honda, Y.; Kitao, O.; Nakai, H.; Klene, M.; Li, X.; Knox, J. E.; Hratchian, H. P.; Cross, J. B.; Adamo, C.; Jaramillo, J.; Gomperts, R.; Stratmann, R. E.; Yazyev, O.; Austin, A. J.; Cammi, R.; Pomelli, C.; Ochterski, J. W.; Ayala, P. Y.; Morokuma, K.; Voth, G. A.; Salvador, P.; Dannenberg, J. J.; Zakrzewski, V. G.; Dapprich, S.; Daniels, A. D.; Strain, M. C.; Farkas, O.; Malick, D. K.; Rabuck, A. D.; Raghavachari, K.; Foresman, J. B.; Ortiz, J. V.; Cui, Q.; Baboul, A. G.; Clifford, S.; Cioslowski, J.; Stefanov, B. B.; Liu, G.; Liashenko, A.; Piskorz, P.; Komaromi, I.; Martin, R. L.; Fox, D. J.; Keith, T.; Al-Laham, M. A.; Peng, C. Y.; Nanayakkara, A.; Challacombe, M.; Gill, P. M. W.; Johnson, B.; Chen, W.; Wong, M. W.; Gonzalez, C.; Pople, J. A. *Gaussian 03*; Gaussian, Inc., Pittsburgh PA, 2003.